13

# Monte Carlo Simulations of Powerful Neutron Interaction with Matter for the Goals of Disclosure of Hidden Explosives and Fissile Materials and for Treatment of Cancer Diseases versus their Experimental Verifications

V.A. Gribkov[1,2,3], S.V. Latyshev[1], R.A. Miklaszewski[2], M. Chernyshova[2], R. Prokopowicz[2], M. Scholz[2], K. Drozdowicz[4], U. Wiącek[4], B. Gabańska[4], D. Dworak[4], K. Pytel[5], A. Zawadka[5], M. Ramos Aruca[6], F. Longo[7], G. Giannini[7] and C. Tuniz[3]

[1]*A.A. Baikov Institute of Metallurgy and Material Sciences, Russian Ac. Sci., Moscow,*
[2]*Institute of Plasma Physics and Laser Microfusion, Warsaw,*
[3]*The Abdus Salam International Center for Theoretical Physics, Trieste,*
[4]*Institute of Nuclear Physics, Polish Academy of Sciences, Krakow,*
[5]*Institute of Atomic Energy, Otwock-Swierk,*
[6]*Institute of Nuclear Science, Miramar # 502, Havana,*
[7]*University of Trieste and INFN, Trieste,*
[1]*Russian Federation*
[2,4,5]*Poland*
[6]*Cuba*
[3,7]*Italy*

## 1. Introduction

One of the most significant task in unveiling of illegal transportation of *explosive or fissile materials*, e.g. inside an airplane luggage, in a car, in a long-distance train carriage or at a sea container, is to disclose of the above illicit materials and explosives *as fast as possible*, probably *during a process of their transportation*.

The method proposed by us lies in a wider group of approaches [1, 2, 3a] that make use of an interaction of neutrons (fast or thermal) with different materials. As a result of such interaction a field of scattered neutrons is formed. This field appears because of elastic and inelastic scattering of primary neutrons by nuclei of irradiated matter. The information on elemental composition of the object can be obtained from spectra of the scattered neutron fields and from amplitudes of peaks corresponding to nuclei of various elements.

The so-called Fast Neutron Scattering Analysis (FNSA) developed lately by Buffler et al. [3*a*] makes use of a train of *nanosecond* pulses of fast neutrons having low intensity (of the order

of $10^2$…$10^3$ neutrons per pulse, supplied by the Van de Graaff accelerator). The necessary data about a chemical content of the substance under interrogation are obtained from an analysis of a spectrum of the *elastically* scattered neutrons registered with a help of a photo-multiplier tube with a scintillator (the time-of-flight – TOF – method). The above authors have demonstrated a possibility to determine relative concentration of the elements H, C, N, and O (very common to different types of explosives) in small (0.2-1.0 kg) samples providing for this goal *a few billions* of the neutron pulses. The main reasons for production of such a huge number of pulses are the necessity to reach exhaustive statistics at the collection of the recoil protons produced by neutrons within a scintillator and to increase a signal-to-noise ratio to a satisfactory level. Other concepts [3*b*...*g*] use also relatively low-intensity (≤ $10^6$…$10^8$ n/pulse) *long-duration* pulses (1-10 μs) generated by neutron sources. They demand many shots during long interrogation time (from few minutes till half an hour with the overall fluence above $10^{11}$ through $10^{13}$ neutrons emitted by the sources in the full solid angle during this examination) and result in high activation of an object under unveiling.

We proposed [6] to bring into play a neutron source based on a *plasma accelerator* of the Dense Plasma Focus type (DPF), which generates pulses of almost monochromatic neutrons of the energy $E_0 \approx 2.5$ or $E_0 \approx 14.0$ MeV with $\Delta E/E_0 \approx 1...3\%$ in the nanosecond (ns) range of their durations but producing at the same time a very large number of neutrons per pulse – $10^8$…$10^{11}$. It gave us an opportunity to provide *all measurements* in TOF technique by means of just a *single* nanosecond pulse, i.e. *during one millionth of a second or less*. Due to the pulse duration used in the proposed method the TOF base can be restricted just by a few meters. The technique that uses a single very bright neutron pulse of nanosecond time duration is named "Nanosecond Impulse Neutron Investigation System" (NINIS).

Our neutron pulse having duration in the range 2...50 ns depending on the DPF size occupies in a space in the direction of its propagation a distance of about 4-50 cm (in fact the neutron pulse from a DPF chamber spreads into space as an almost spherical shell of the above thickness). This distance is approximately the same as the distance of neutron's penetration depth into suspicious materials (e.g. explosives). Because of the unique characteristics of the neutron source the *signal-to-noise ratio* will be increased just proportionally to the decreased number of shots (e.g. one pulse instead of billions compared with the case of the Van de Graaff source [3a]) whereas *neutron fluence* necessary to characterize hidden objects will be reduced by 2-4 orders of magnitude compared with [3]. It results in low activation of items under interrogation.

However, for this very promising technique to be proved theoretically and then verified experimentally it is needed to provide a very accurate preliminary numerical modeling of neutron scattering in real geometries. Sometimes (in particular in the cases of *inelastic* scattering of neutrons by *fissile* materials – see below) we have to know the resulted spectrum beforehand. These simulations can be produced with the help of Monte-Carlo codes.

## 2. Numerical modeling of the NINIS method by use of MCNP5 and FLUKA codes

We applied MCNP™ – a general-purpose Monte Carlo N-Particle code that can be used for neutron, photon, electron, or coupled neutron/photon/electron transport calculations [4] (MCNP, MCNP5, and "MCNP Version 5" are trademarks of the Regents of the University of California, Los Alamos National Laboratory). The code treats an arbitrary three-dimensional

configuration of materials in geometric cells bounded by first- and second-degree surfaces and fourth-degree elliptical tori. Pointwise cross-section data are used. For neutrons, all reactions given in a particular cross-section evaluation (such as ENDF/B-VI) are accounted for. Thermal neutrons are described by both the free gas and S(α, β) models. Important standard features include a powerful general source; both geometry and output tally plotters; a rich collection of variance reduction techniques; a flexible tally structure; and an extensive collection of cross-section data.

We undertake attempts to simulate scattering of 2.45-MeV neutrons from various objects by means of full MCNP calculations. We used MCNP5 [4b], the 5-th version of the MCNP, which takes into account the whole process of neutron scattering by dissimilar objects and allows to model signals registered by virtual detectors with high precision. As an example we present here usage of this MCNP5 code to simulate scattering of neutrons from *long objects* (Fig.1).

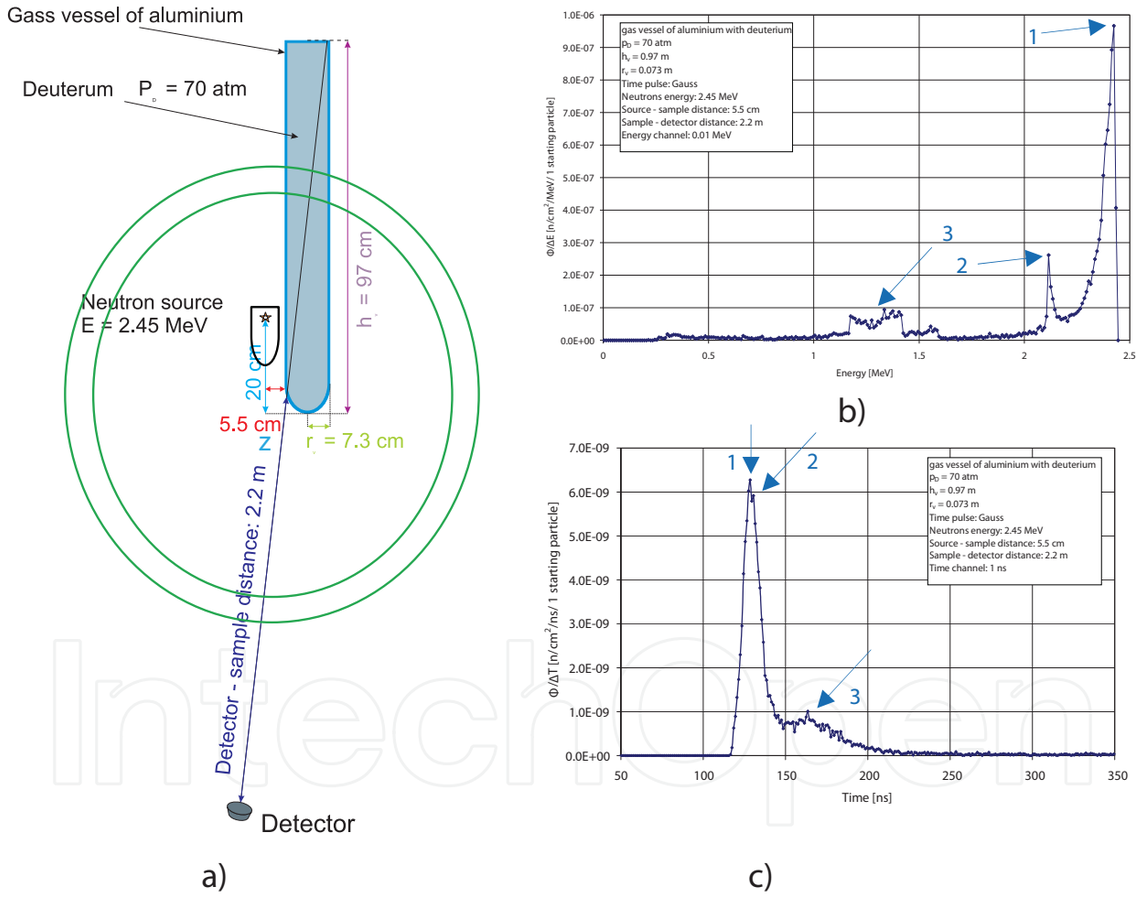


Fig. 1. Scheme of numerical experiment (*a*), energetic distribution (*b*) and temporal behaviour (*c*) of neutrons coming to the detector: 1 – direct neutrons (2.45 MeV), 2 – neutrons scattered by aluminium, 3 – neutrons scattered by deuterium

In this picture there is a scatterer – a 1-meter high-pressure aluminium cylinder filled with deuterium at 70 atm. – and a DPF-based neutron source (Fig. 1a). The energy distribution (spectrum) of "direct" and scattered neutrons is presented in Fig. 1b whereas the resulting time-of-flight signal (the expected oscilloscope trace) is shown in Fig. 1c.

These our computational works were aimed also at elaboration of the theoretical basis for the *fissile materials detection concept* and to verify expected experimental results.
The first part of them applies a FLUKA code [5] to investigate detailed interaction of neutrons with localized objects (explosives and fissile materials as well as everyday use materials). The FLUKA code is described further in the text. The calculations were provided in the idealized geometry shown in Fig. 2.
Neutrons from DPF irradiate the target (a fission fuel element) as a parallel beam along Z-axis. The beam has a diameter 7 cm which is equal to the diameter of the fuel element. The target was *a fuel element MR-6/80%*, which consists of 6 concentric tubes (internal tube in some calculations was substituted by a rod made of aluminium). The area of the cross-section of the neutron beam is 38 $cm^2$. The total area of the whole fission fuel element is 7 cm × 100 cm = 700 $cm^2$. Thus the neutron beam irradiates only a small part of the overall fuel element.
Neutrons and X-Ray photons are registered on the surface of a sphere surrounding the target and having a radius equal to 200 cm. The sphere is divided into zones occupied by detectors. Each zone has a width equivalent to 20 cm. Thus all detectors are "seen" by particles escaping the target within the same angle equal to 5.73° except the last detector #32 (backside of the neutron beam), which has the angle of particles' collection slightly higher.

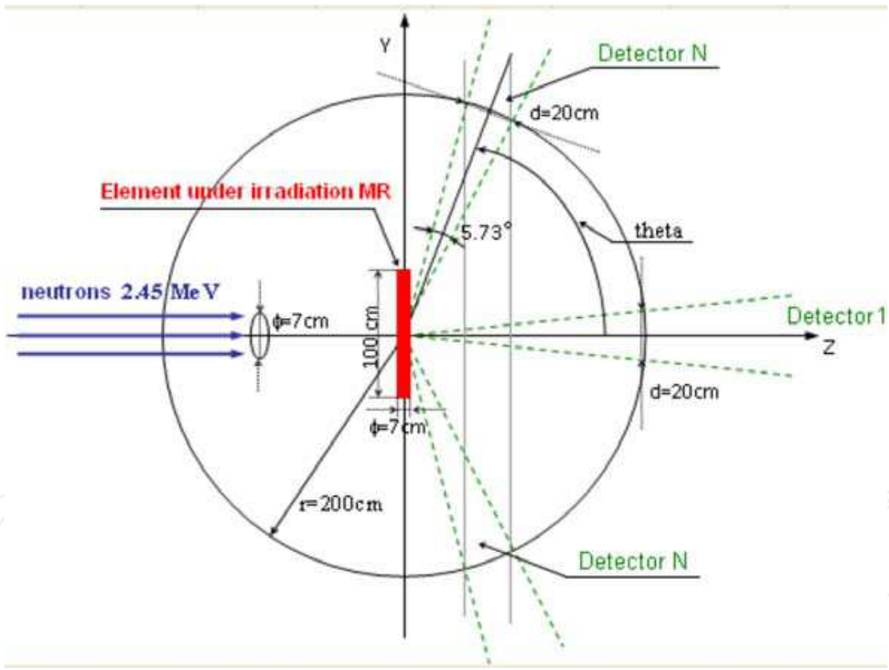


Fig. 2. Idealized geometry of the neutron beam and positioning of a sample under irradiation and neutron detectors

Below we present a table contenting results of our calculations and two pictures (Fig. 3 *a* and *b* correspondingly) demonstrating one example of energy distributions of neutrons and photons escaping the target at a certain angle (i.e. for a certain detector) after irradiation. Solid line in red color shows results for original fuel elements MR. Green dashed line presents results obtained for pure aluminium, i.e. at the substitution of uranium fuel layers by aluminium layers to show clearly an effect of the „aluminium background". Boundary

energy is energy of the irradiating neutron beam, above which every neutron originates only from fission of uranium in the fuel layer. Due to this feature fission neutrons are seen especially clear.

FNSA-2009: Fuel element MR-6/80% placed perpendicularly to the beam of 2.45-MeV neutrons. Number of simulated histories – 100 mln of neutrons from the source.
Estimator: Boundary crossing absolute FLUENCE one-way estimator

| DET | theta [deg] | Neutrons (*) | Photons (*) | N<2.466 (*) | N>2.466 (*) | %N>2.466 [%] |
|---|---|---|---|---|---|---|
| 1 | 0.00 | 2.19E-03 | 1.74E-07 | 2.19E-03 | 3.37E-09 | 1.54E-04 |
| 2 | 5.73 | 5.62E-07 | 1.73E-07 | 5.59E-07 | 2.97E-09 | 5.28E-01 |
| 3 | 11.46 | 3.29E-06 | 1.72E-07 | 3.29E-06 | 2.89E-09 | 8.77E-02 |
| 4 | 17.20 | 1.81E-06 | 1.70E-07 | 1.81E-06 | 2.80E-09 | 1.54E-01 |
| 5 | 22.93 | 6.44E-07 | 1.69E-07 | 6.41E-07 | 2.80E-09 | 4.35E-01 |
| 6 | 28.66 | 3.68E-06 | 1.70E-07 | 3.67E-06 | 2.79E-09 | 7.59E-02 |
| 7 | 34.39 | 6.88E-07 | 1.69E-07 | 6.85E-07 | 2.77E-09 | 4.02E-01 |
| 8 | 40.12 | 3.12E-07 | 1.67E-07 | 3.09E-07 | 2.87E-09 | 9.20E-01 |
| 9 | 45.86 | 2.27E-06 | 1.66E-07 | 2.26E-06 | 2.82E-09 | 1.24E-01 |
| 10 | 51.59 | 5.84E-07 | 1.65E-07 | 5.82E-07 | 2.73E-09 | 4.68E-01 |
| 11 | 57.32 | 7.10E-07 | 1.62E-07 | 7.07E-07 | 2.82E-09 | 3.98E-01 |
| 12 | 63.05 | 8.47E-07 | 1.59E-07 | 8.44E-07 | 2.75E-09 | 3.25E-01 |
| 13 | 68.78 | 7.26E-07 | 1.56E-07 | 7.23E-07 | 2.65E-09 | 3.66E-01 |
| 14 | 74.52 | 3.94E-07 | 1.52E-07 | 3.91E-07 | 2.64E-09 | 6.71E-01 |
| 15 | 80.25 | 4.22E-07 | 1.47E-07 | 4.19E-07 | 2.50E-09 | 5.92E-01 |
| 16 | 85.98 | 4.49E-07 | 1.43E-07 | 4.46E-07 | 2.43E-09 | 5.42E-01 |
| 17 | 91.71 | 3.09E-07 | 1.42E-07 | 3.06E-07 | 2.44E-09 | 7.90E-01 |
| 18 | 97.44 | 3.16E-07 | 1.46E-07 | 3.14E-07 | 2.46E-09 | 7.79E-01 |
| 19 | 103.18 | 3.48E-07 | 1.51E-07 | 3.46E-07 | 2.63E-09 | 7.54E-01 |
| 20 | 108.91 | 2.92E-07 | 1.55E-07 | 2.90E-07 | 2.61E-09 | 8.93E-01 |
| 21 | 114.64 | 1.70E-07 | 1.59E-07 | 1.67E-07 | 2.70E-09 | 1.59E+00 |
| 22 | 120.37 | 2.47E-07 | 1.62E-07 | 2.44E-07 | 2.74E-09 | 1.11E+00 |
| 23 | 126.10 | 5.93E-07 | 1.65E-07 | 5.90E-07 | 2.78E-09 | 4.69E-01 |
| 24 | 131.84 | 2.67E-07 | 1.67E-07 | 2.64E-07 | 2.77E-09 | 1.04E+00 |
| 25 | 137.57 | 2.36E-07 | 1.68E-07 | 2.33E-07 | 2.89E-09 | 1.22E+00 |
| 26 | 143.30 | 2.16E-07 | 1.70E-07 | 2.14E-07 | 2.71E-09 | 1.25E+00 |
| 27 | 149.03 | 6.62E-07 | 1.70E-07 | 6.60E-07 | 2.75E-09 | 4.15E-01 |
| 28 | 154.76 | 3.33E-07 | 1.73E-07 | 3.30E-07 | 2.88E-09 | 8.66E-01 |
| 29 | 160.50 | 3.76E-07 | 1.73E-07 | 3.73E-07 | 2.94E-09 | 7.82E-01 |
| 30 | 166.23 | 7.01E-07 | 1.74E-07 | 6.98E-07 | 2.97E-09 | 4.24E-01 |
| 31 | 171.96 | 4.04E-07 | 1.73E-07 | 4.01E-07 | 2.88E-09 | 7.12E-01 |
| 32 | 180.00 | 8.42E-07 | 1.76E-07 | 8.39E-07 | 3.13E-09 | 3.71E-01 |

(*) – units: [particles/cm$^2$/one beam neutron]
N<2.466 – number of neutrons with energy E<2.466 MeV (lower limit of energy of beam neutrons)
N>2.466 – number of neutrons with energy E>2.466 MeV (unambiguously coming from fission)
%N>2.466 – percentage of neutrons having energy E>2.466 MeV (ratio of columns 6 to 3)

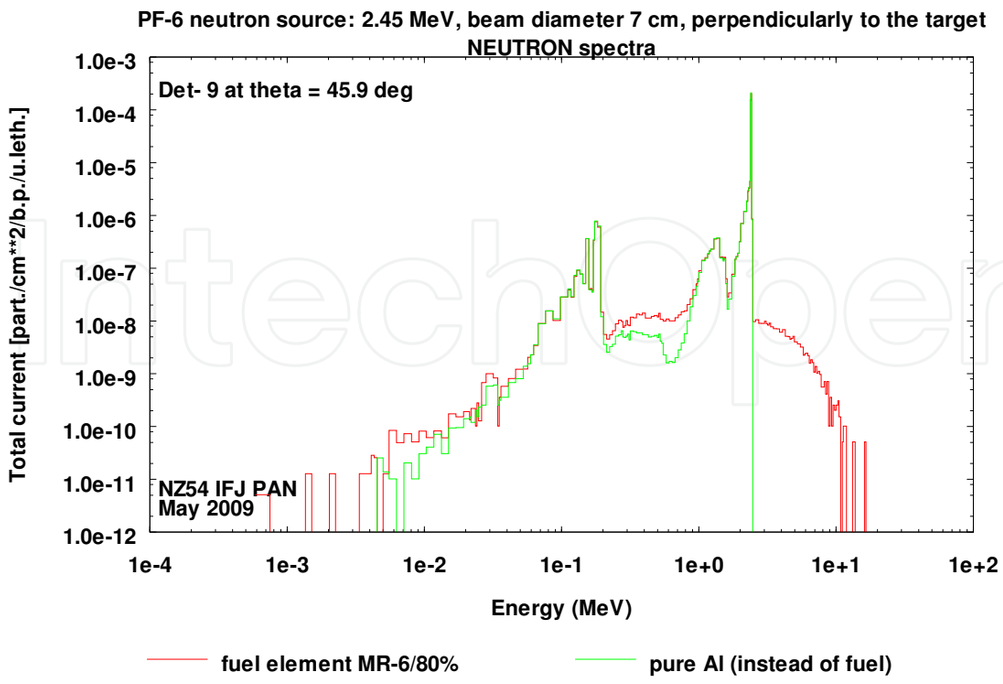


a)

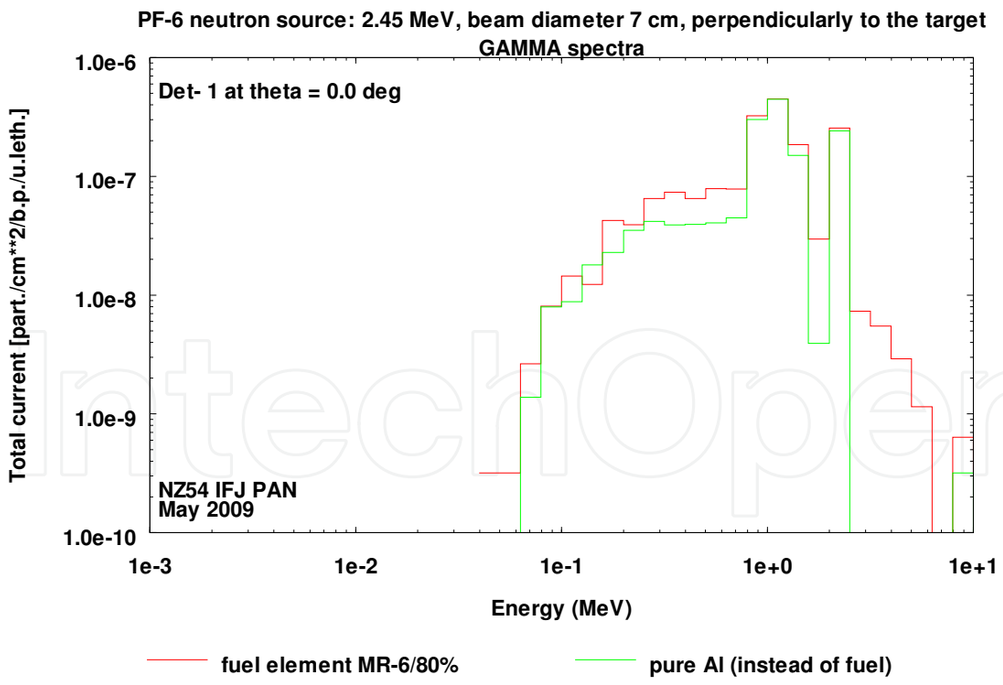


b)

Fig. 3. Number of neutrons and gamma-photons produced due to fission processes in the fuel element MR-6/80% (red colour); note neutrons whose energy exceeds the energy specific for the DPF device (on the right-hand side)

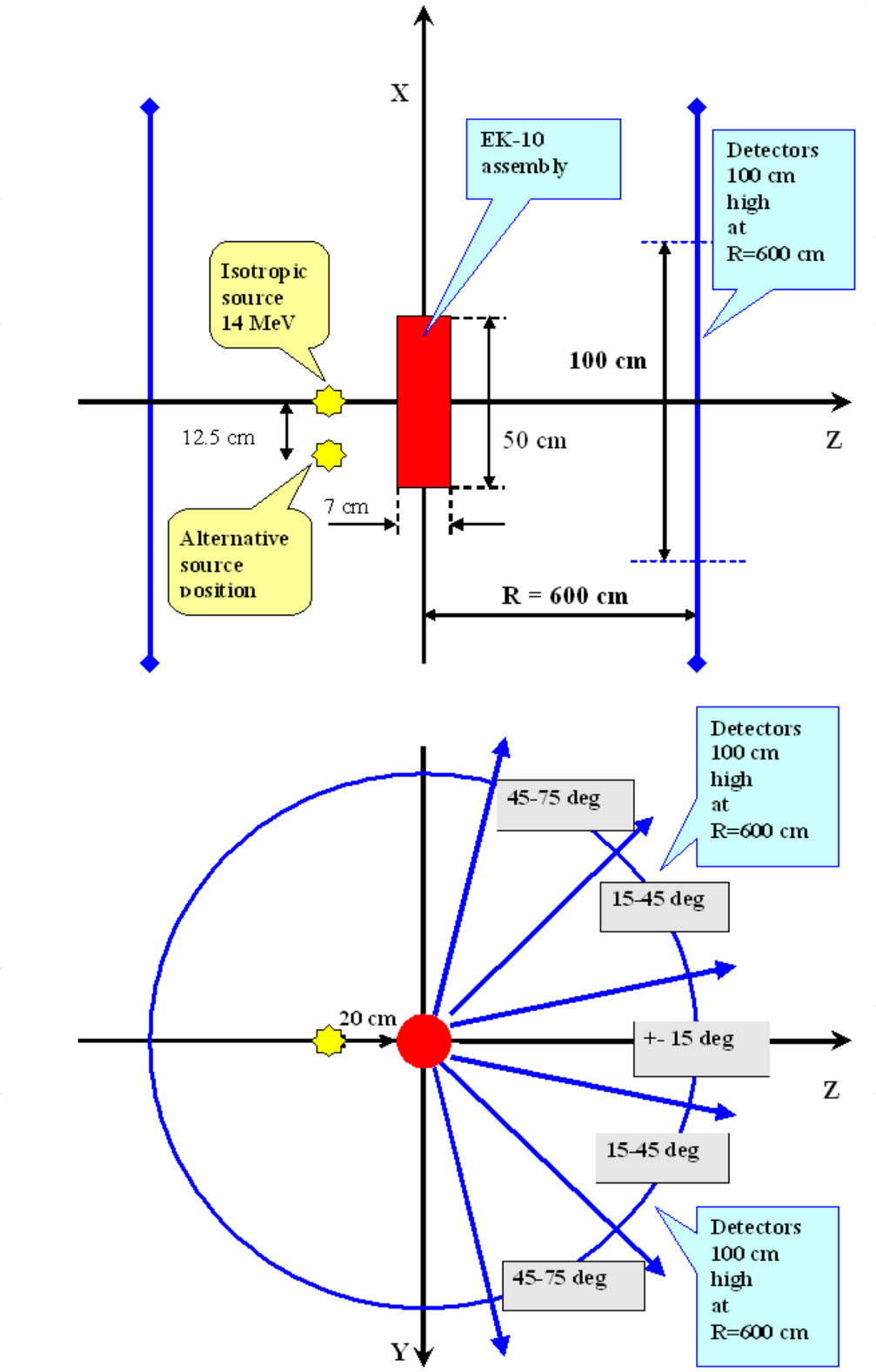


Fig. 4. Geometry of the experiment for 14-MeV neutrons irradiating fuel element EK-10

One may see that the number of fission neutrons may amount a few percent of the "low-energy" scattered neutrons. However taking into consideration that our DPF devices (PF-6 [4]) can produce neutron yield for $E_0$ ~ 2.466-MeV neutrons (i.e. operating with pure deuterium as a working gas) on the level $10^9$ neutrons per pulse only, one may see that the number of high-energy (i.e. fission) neutrons coming to the detector's scintillator that has a 10-cm width in the above idealized geometry under consideration (Fig. 2) is not high enough to be detected them confidently. Thus we have to come to shorter distances between the DPF-based neutron source and the fuel element (compared with the above 2 meters), to wider neutron beams. Also we must use 14-MeV neutrons from DPF operated with DT mixture as a working gas. In this configuration the total neutron yield of PF-6 in a single shot is two orders of magnitude higher for this device ($10^{11}$ n/pulse). However in this case spectrum of fission neutrons will have energies less compared with the energy of primary, i.e. 14-MeV neutrons.

Thus the next step in our simulation works was done in geometry (Fig. 4) more close to our real experiments produced with the PF-6 device and described below. The device was operated in the experiments with the DT-filled chamber.

With this geometry we provided numerical modelling by use of the FLUKA code again. This code has been developed for many years at CERN and Milan. The code distinguishes "high energy neutrons" and "low energy neutrons". The border is at 20 MeV. All neutrons with energy lower than 20 MeV are called "low-energy neutrons" and they are calculated separately and differently than other particles. To solve these low-energy neutron transport problems FLUKA applies the so-called multigroup method. This widely known approach is similar to that applied in famous MORSE MC code – one of the progenitors of modern MC calculations in radiation transport. In the case of FLUKA the whole low-energy neutron range, starting from neutron energy $E$ = 20 MeV down to $E$ = 1.0E-5 eV, is divided into 260 neighbouring, contiguous energy groups. Afterwards, due the course of calculations we don't say about neutron energy but rather about neutron group. In this way energy of each neutron is determined with accuracy to the group limits. Group numbers go always in descending mode (bigger group no. means lower energy). The TOF spectra are obtained by simple recalculation of neutron energies to time of flight – for distance 6 m in this case.

In this modelling the source is very simple. It is mono-energetic (14 MeV), point, instant, and fully isotropic source. For this reason one cannot observe in the spectra a peak at 2.45 MeV originated from the D-D reaction taking place inside the DPF chamber and seen in the real oscilloscope traces (see below).

Generally speaking the code doesn't distinguish elastic and non elastic collisions. All this information is included in the so-called transfer matrix. For each material (nucleus) the transfer matrix includes integrated cross-sections for all energy groups – recalculated to probabilities. Simply speaking, for each material and neutron energy group the probability distribution exists. These probabilities say: what is the chance that after a collision a neutron falls down into a given group. In other words, from this distribution the final (after collision) neutron group is sampled. Sampling of fission neutrons is made additionally after collision with fissionable materials. If we have a mixture of many nuclei a neutron chooses the nucleus for interaction on the base of total, macroscopic cross-sections.

*Fuel assembly EK-10*

Fuel composition is mixed $UO_2$ and Mg (73.33g of U-238, 8.05g of U-235, 13.03g of Mg).

An individual fuel element is a cylinder: 50 cm high and 7 mm in diameter, which makes 19.24 $cm^3$ of the total volume.

| Element | Atomic number | Atomic weight [u] | Proportion by number [%] | Proportion by weight [g/cm$^3$] |
|---|---|---|---|---|
| U-235 | 92 | 235.044 | 2.19 | 0.4184 |
| U-238 | 92 | 238.051 | 19.71 | 3.8113 |
| O | 8 | 15.999 | 43.80 | 0.5693 |
| Mg | 12 | 24.305 | 34.30 | 0.6772 |

Fuel density: 5.4762 g/cm$^3$

Fuel *assembly* was modelled as 16 cylindrical fuel pipes. Each pipe is 50 cm high and has an external diameter equal to 10 mm (7 mm of fuel + 2 x 1.5 mm of aluminium wall). The pipes are parallel to each other and they form sort of a ring bundle. Looking at the bundle cross sections (at YZ plane) the centres of these 16 pipes are on the ring with diameter 6 cm, and go around, thus the pipes are almost close to each other. In this way we can say that the „external diameter" of this ring of the pipes (whole assembly) is equal to 7 cm (and internal diameter 5 cm). Fig. 5 shows results of these calculations for spectra of 14-MeV neutrons scattered by several elements composing the fuel element.

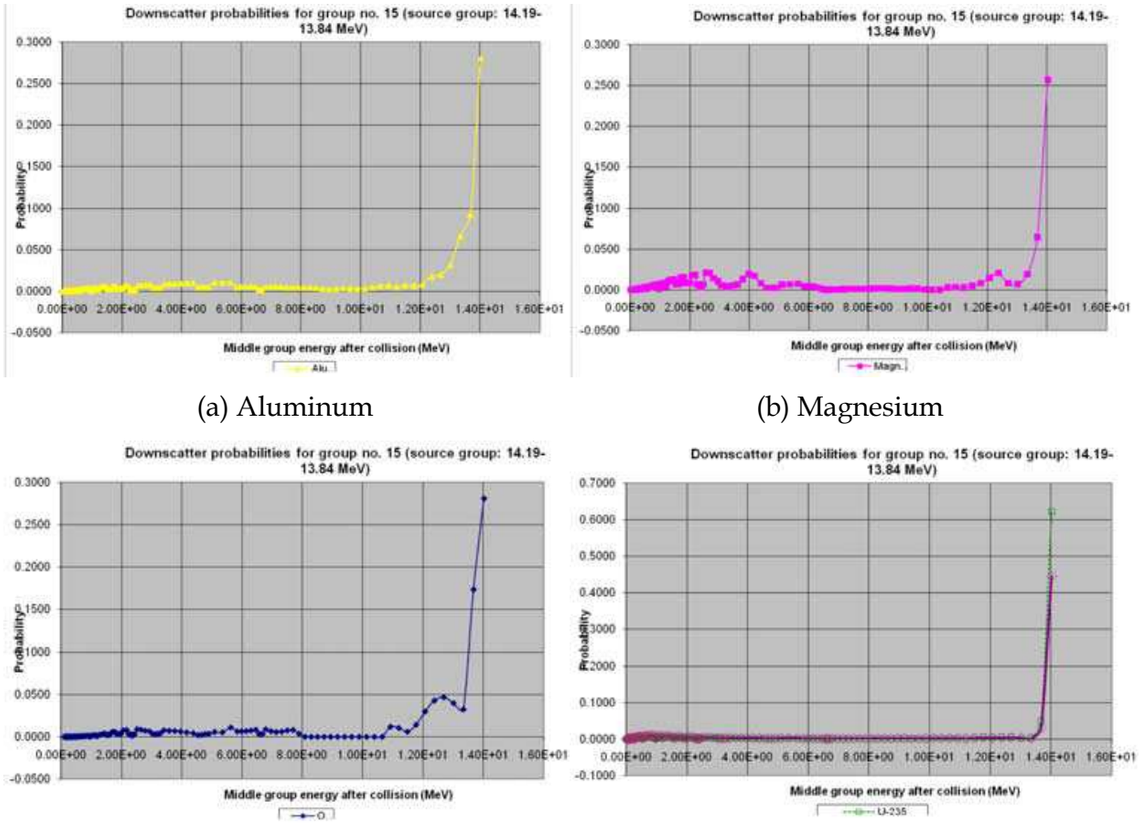


(a) Aluminum (b) Magnesium

c) Oxygen d) Uranium U-235 (□) and U-238 (○)

Fig. 5. Results of FLUKA-code calculations for spectra of 14-MeV neutrons scattered by several nuclei composing the fuel element

In the below results of calculations one may see peaks at different energies specific for each element's nucleus. Vast majority of neutrons are scattered *elastically* by the elements, and

this peak merges with the main peak of primary neutrons: after scattering in given material, for instance Oxygen, of a neutron in energy group 15, the probability of getting a neutron in the same group (15) is 28.10%; that to get a neutron in the following group (group 16) is 17.34%, in group 17 it is 3.25% etc.
In Fig. 6 one may see spectrum of neutrons scattered on uranium nuclei with an enlargement of the region where we have to have our inelastically scattered (fission) neutrons (with spectrum centred near 0.5…1.5 MeV).

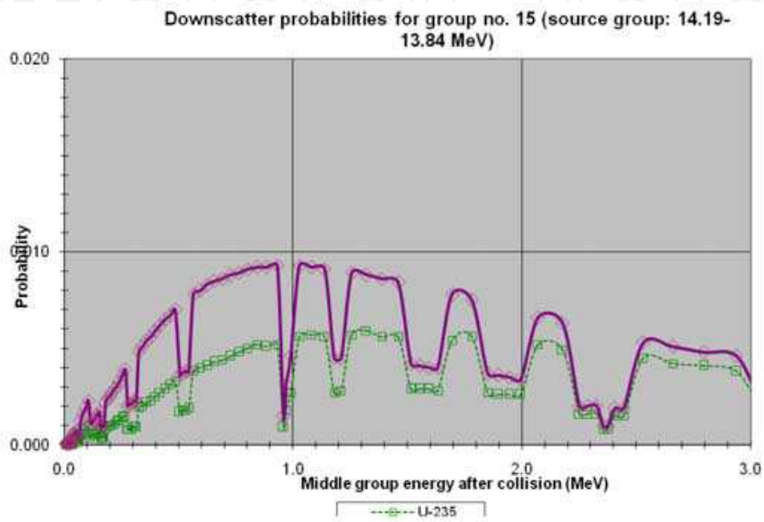


Fig. 6. Spectrum of neutrons scattered by uranium nuclei U-235 (□, green) and U-238 (◊, violet)

## 3. Tests of NINIS technique – "proof-of-principle" experiments

a. For a verification of our MCNP simulations we provide in our first session a *"proof-of-principle" experiment* investigating scattering of neutrons by 1-liter bottles of ethanol ($C_2H_5OH$) [6], methanol ($CH_3OH$) and phosphoric acid ($H_3PO_4$) positioned in a very close vicinity to the DPF chamber. The geometry of the experiment is shown in Fig. 7.

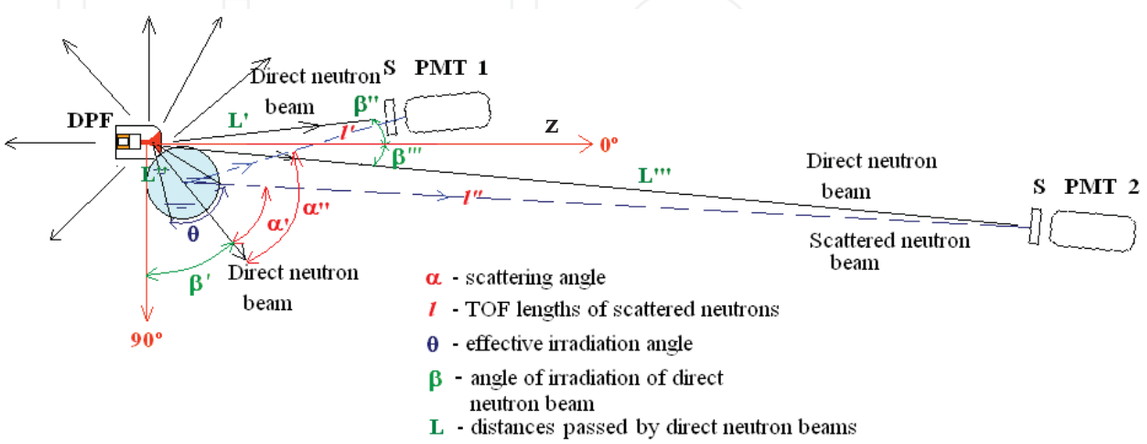


Fig. 7. Scheme of the "proof-of-principle" experiments

In the first cases we used in PF-6 the discharge chamber producing $10^9$ of 2.45-MeV neutrons per shot ($E_{bank}$ = 7 kJ) whereas later we operated with the DPF bank energy on the level of about 4-5 kJ with neutron output of the device ~ $3\times10^8$ neutrons per pulse. Our scintillator used for the PMT probe had a diameter 10 cm with its length of 10 cm. Our fast channels (photomultiplier tubes with scintillators – PMT+S) had in these experiments temporal resolution 3.12 ns. We used two channels placed in $L'$ = 1.0-m and $L''$ = 18.5-m distances from the DPF. A typical result obtained with them for the second case is presented in Fig. 8. The lowest trace is the same as the middle one but taken with a higher sensitivity of the oscilloscope.
Preliminary testing shots made with the PF-6 device (IPPLM) have shown that the hard X-Ray pulse (HXR, photon energy $h\nu$ > 60 keV) always has its rise-time shorter than the temporal resolution of our PMT+S channels.

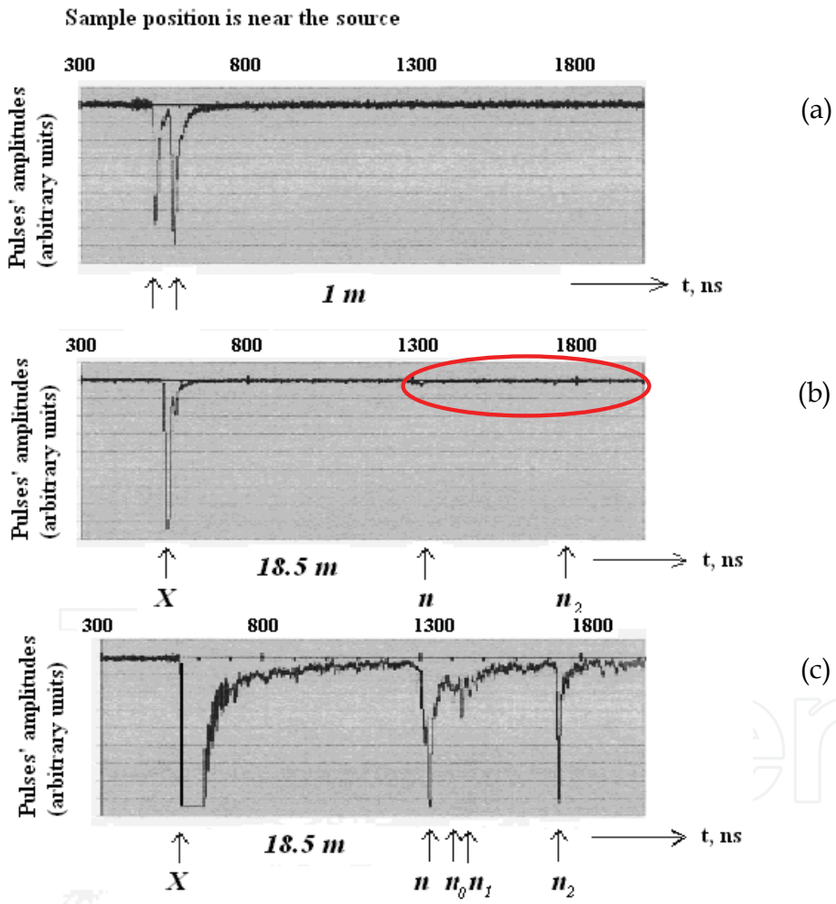


Fig. 8. Oscilloscope traces of PMTs placed at 1.0 and 18.5 meters from the target

At the same time a set of 100 successive shots made during this experiment simultaneously with two PMT+S placed at 3.5 and 7.5 meters from the DPF chamber in the same direction (along Z-axis) has shown that *inside the chamber* the neutron pulse follows the HXR pulse with the delay of 8 ns +/- 2 ns [6]. And what's more, the broadening of the same neutron pulse at the distance of 7.5 meters compared to the pulse measured at 3.5 meters shows that the neutron spectrum in Z-axis direction is monochromatic: $\Delta E/E \approx 1\ldots3\%$.

In the oscilloscope trace of Fig. 8 (*c*) for the PMT+S positioned at 18.5-m distance a sequence of pulses is seen, which demonstrates different energies because of their delay time in relation to the hard X-Ray pulse.

First of all a calculation of neutrons' energy of the first pulse ("*n*"), seen in Fig. 8 and provided by use of time-of-flight (TOF) data with the help of formula:

$$E\ [\text{MeV}] = (L[\text{m}] / t\ [\text{ns}])^2 \times 5.23 \cdot 10^3,$$

has shown that the medial magnitude of the energy of these neutrons is ≈ 2.6 MeV. This value is a typical one for neutrons generated in a DPF in forward direction, i.e. with the small angle in relation to Z-axis of its chamber ("head-on" neutrons). However the so-called "side-on" neutrons generated at the angle 90° to Z-axis of a DPF chamber have energy 2.45 MeV.

To calculate the real position of neutron pulses "$n_0$" and "$n_1$" in the oscilloscope trace and consequently their TOF and energy we have to perform the following procedures:

1. To move to the left on the oscilloscope trace the hard X-Ray pulse by its TOF of 18.5 m (62 ns). It will be the moment of the appearance of the HXR pulse inside the chamber.
2. To move to the right on the oscilloscope trace the above point by 8 ns – it will be the moment for neutrons to top out their maximum inside the DPF chamber.

After the above procedure we shall have the *reference point*, from which we can calculate all time intervals needed for direct or scattered beams of neutrons to reach our PMT. Taking into consideration that our target is placed at a distance of 20 cm to the DPF chamber center and in the "side-on" position, we have to perform all calculations for the neutrons *having energy 2.45 MeV* and in the conditions that their direct TOF from the centre of the DPF chamber till the target is 10 ns. Effective angle of the bottle's irradiation was $\theta \approx 10^o$.

Kinematics of elastic scattering of neutrons by different nuclei gives the diagram of the dependence of lost energy at collisions in relation to the neutron laboratory scattering angle (Fig. 9).

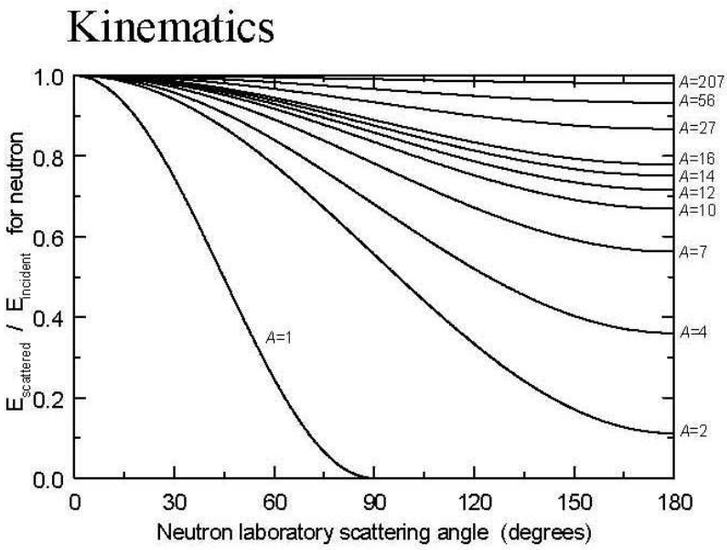


Fig. 9. Graph showing the ratio of energy of neutrons scattered by nuclei of various elements to the initial energy of neutrons of the irradiating beam in dependence of scattering angle

Our PMT+S probe was placed at the angle $\alpha$ of about 80° to the direction of the neutron beam passing through the centre of the bottle with methanol. From kinematics of scattering and in our experimental geometry one can see that our two peaks on the oscilloscope trace – "$n_0$" (908 - 10 = 898 ns) and "$n_1$" (925 - 10 = 915 ns) – may be attributed to the scattering of the *2.45-MeV neutrons* on the *oxygen* and *carbon* nuclei accordingly (Fig. 10). Uncertainty is resulted from neutron pulse's duration ($\tau$), time resolution of detectors, from a precision of measurements of the peak's position on the trace, and due to TOF of neutrons through the bottle. It shows that in principle scattering on nitrogen nuclei can be distinguishable in this experiment as well.

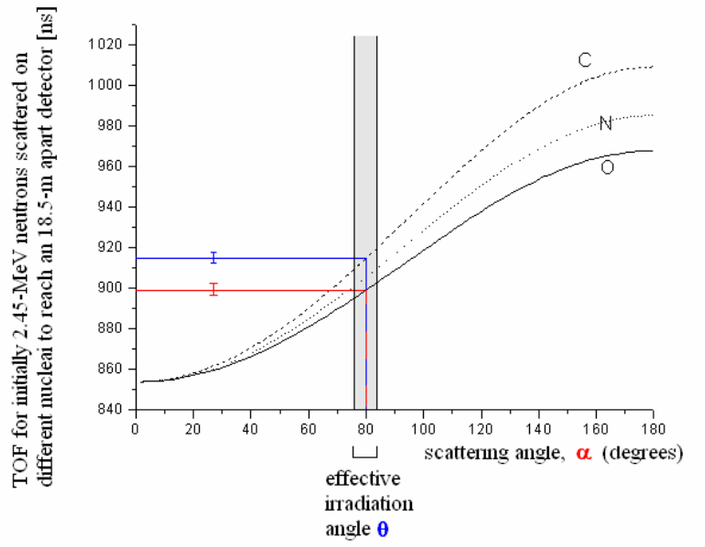


(a)

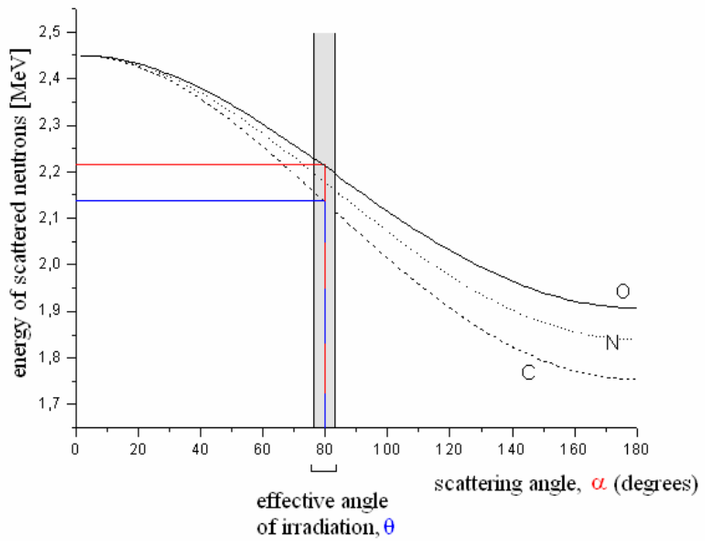


Fig. 10. TOF for 18.5 m (*a*) and energy (*b*) measurements plotted for the scattering scheme presented in Fig. 7

It appears also that our high-pressure 10-litre 1-m by height cylinder made of aluminium and filled with deuterium at a *high pressure* ≈ 150 atm. is responsible for "$n_2$" pulse. It was placed at 1 m from the DPF chamber. It has rather *small diameter* of about 14 cm (less compared with the space occupied by the neutron pulse in the propagation direction) and it was positioned *vertically* that resulted in a short scattering pulse.

It is interesting to compare cross-sections of 2.45-MeV neutrons, elastically scattered by nuclei of the above materials, and of 2.6-MeV neutrons – on a 20-cm *Teflon* cylinder (positioned in the direction of the PMT+S and blocking neutrons i.e. forming a sort of a "screen" for the strait-forward beam of neutrons). It appears that this figure is equal to 1.5 barns for nuclei of $^{12}C$, whereas the related magnitude for $^{16}O$, which is going to a minimum at 2.35 MeV (relatively narrow) in this range of $\sigma(E)$ is equal to 0.6 barns at its slope. Cross-sections of elastic scattering on deuterium and aluminium are 2.35 and 2.2 barns correspondingly. For fluorine and 2.6-MeV neutrons it is on the level of 1.5 barns. These figures together with the geometrical factors and chemical formulas of the substances under irradiation are very well fitted to the relative ratio for the amplitudes of the peaks "$n$", "$n_0$", "$n_1$", and "$n_2$".

b. Our next experiment was devoted to the clarification of the *restrictions of the method implied by distances and neutron yield* of the device. A 1-litre bottle with phosphoric acid ($H_3PO_4$) was used as a target in this very case. Diameter of the bottle was 10 cm. It was installed tightly with the DPF chamber, and the geometry of our experiments was the same as above with $\beta' \approx 35°$, $\beta'' \approx \beta''' \approx 27°$, $L' = 2.2$ m, $L'' = 8$ cm, $\theta \approx 10°$, $L''' = 7$ m. In these tests we have experienced an opportunity to use much lower bank energy (~2…3 kJ), smaller DPF chamber, and decreased neutron yield (~ $10^8$ n/shot) which results in much lower activation of objects under interrogation and in shorter TOF base as well (2.2 meters). We used here 2 PMT of the SNFT type (2.5 ns time resolution) placed in two different distances from the scatterer in each experiment. In this case the neutron pulse duration detected at a close vicinity to the DPF chamber became 5-8 ns. Thus the longitudinal dimension occupied by the pulse in the direction of its propagation (or a "thickness" of an almost spherical neutron "shell" spreading from the DPF chamber into space) is about 10-15 cm.

Two typical oscilloscope traces taken at the experiments with a bottle of phosphoric acid obtained from S+PMT-1 for two different situations – when direct neutron beam to the PMT-1 from the DPF chamber was almost completely blocked by a screen and conversely when it irradiated a scintillator freely – are shown accordingly in Fig. 11 *a* and *b*.

Because the neutron detector signals contain an essential noise component in this case of a low dose of neutrons we used a Wavelet method suggested by MATLAB Wavelet Toolbox. We used De-noising 1-D. We considered the noise to be un-scaled white. The signal was presented by 2048 numerical points. We used soft fixed form of the threshold method. Fig. 11 *c* and *d* shows the de-noising of the signals, where a number of wavelets were used for real oscilloscope traces *a* and *b*. Different variants of wavelets give the same result with good accuracy. Thus one can see that the results of the wavelet de-noising allow identifying reliably peaks 1, 2, and 3. Same procedure as above has shown that peaks 2 and 3 belong to neutrons scattered by nuclei of phosphorus and oxygen.

Taking into account cross-sections and number of atoms in the acid's molecule we have verified why both peaks are almost equal by their amplitudes (difference is 1.2 times). Of course, to compare these amplitudes one has to subtract background from the overall signal as it is shown by vertical bars (red lines) in Fig. 11 *c* and *d*. Thus these sets of tests has shown

that even ~ $10^8$ neutrons per pulse and TOF base equal to about 2 meters can still serve in certain cases in our NINIS technique.

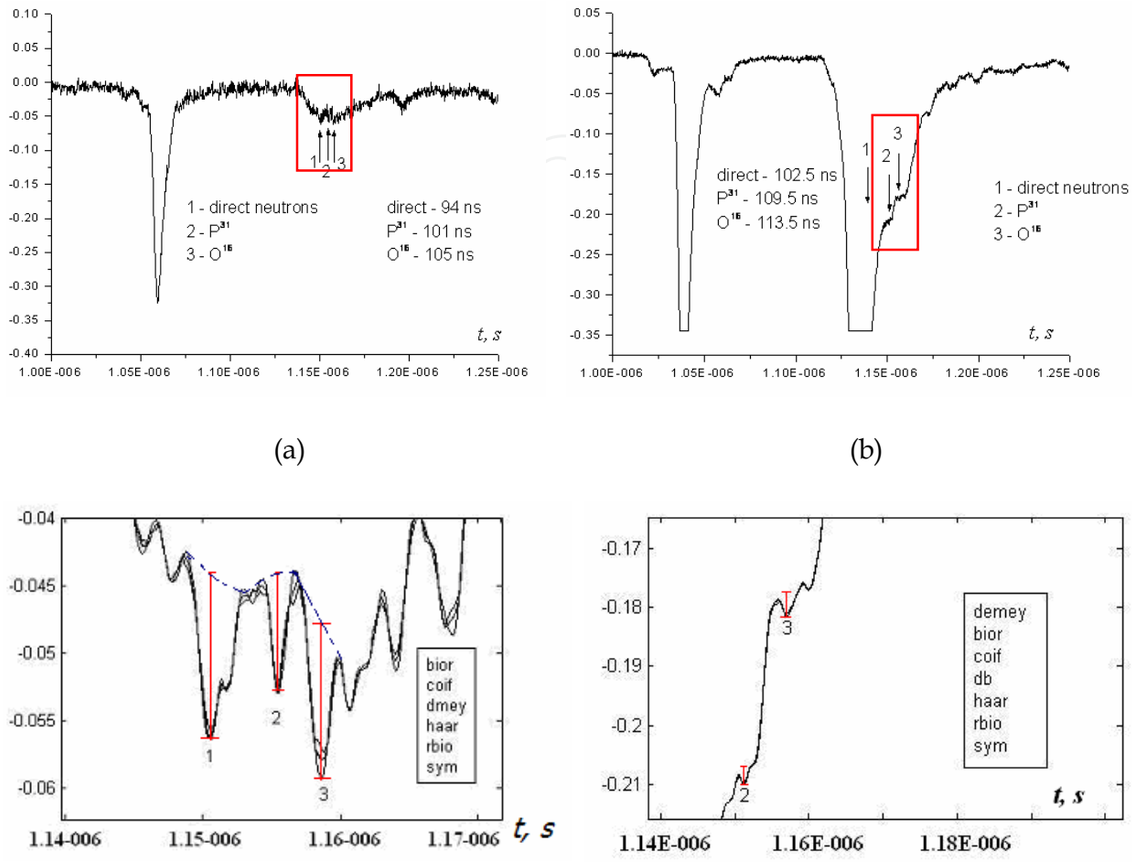


(a) (b)

(c) (d)

Fig. 11. Oscilloscope traces for the cases when direct beam of neutrons (1) was blocked almost completely by a neutron screen (*a*) and without screening (*b*); de-noising signals obtained with different wavelet types, level 2: (*c*) for (*a*) and (*d*) for (*b*)

c. Our next experimental session was devoted to *lengthy objects*. We used our high-pressure cylinder made by aluminium and filled with deuterium with the pressure of 70 atm. in this case. The geometry of the experiment was the same as shown in our MCNP simulations (Fig. 1a). Typical oscilloscope traces are shown in Fig. 12.

Difference in time lags between these experimental results and our simulation oscilloscope trace (Fig. 1c) is small. It comes from the fact that in our numerical modeling we supposed that DPF irradiates 2.45-MeV neutrons in *all* directions. In our real situation neutrons irradiated along Z-axis have energy 2.6 MeV. That is why they come to the detector slightly earlier. It is clearly seen also that the pulse of neutrons, scattered by deuterium, has the *same rise-time* as the neutron pulse from DPF. However it obeys *much longer tail* compared with the pulse of direct neutrons. It comes from the fact that the length of our object (~ 1 m) is about 4-5 times *higher* compared with the "thickness" of our neutron shell (≈ 20 cm).

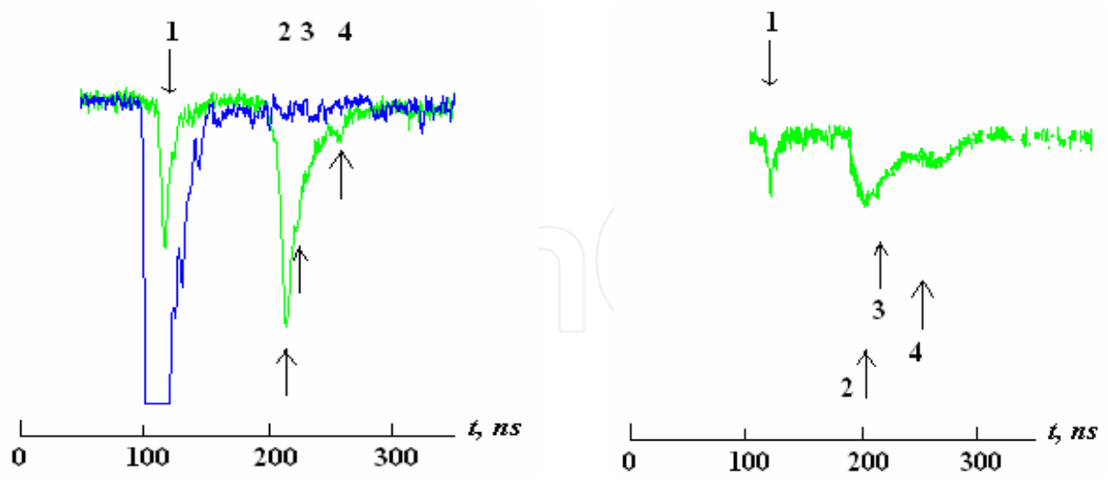


(a) (b)

Fig. 12. Oscilloscope traces without a screen (a) and with it (b) blocking partially X-Rays (1) and direct neutrons (2) but not blocking neutrons scattered by Al (3) and $D_2$ (4) nuclei

Mean free path (MFP) of neutrons in deuterium at 70 atm. is:

$$L_D = 1/n\sigma = 1/2\times2\times2.7\times10^{19}\times70\times2.3\times10^{-24} \approx 100 \text{ cm},$$

where $L_D$ – *MFP*, $n$ – nuclei (atoms) concentration in 1 $cm^3$, $2.7\times10^{19}$ – Loschmidt's number, pressure $p$ = 70 atm, and $\sigma$ – cross-section of elastic scattering, i.e. $L_D$ is about the length of our high-pressure cylinder $l$ = 1 m. Thus this short single-pulse technique can characterize *geometry of objects*.

At the same time the pulse of neutrons scattered by aluminium wall of the cylinder is short. It reflects the fact that our PMT+S was oriented *along* the cylinder's wall, so neutrons scattered by the most distant part of the aluminium wall were *absorbed* by closer parts of it. Indeed the MFP of 2.45-MeV neutrons in aluminium is 20 cm:

$$L_{Al} = 1/n\sigma = 1/1.7\times10^{22}\times3\times10^{-24} \approx 20 \text{ cm},$$

with $n = \rho/u\times m_p = 2.7/27\times1.67\times10^{-24}$, where $\rho$ – specific density of aluminium, $u$ – unified atomic mass unity, $m_p$ – proton's mass. So MFP here is much less compared with the cylinder length: $L_{Al} << l$. Thus our detector shows the neutrons scattered only by the part of the cylinder closest to the detector. However this MFP value in aluminium is about the same as the "thickness" of our neutron shell.

d. In the next session we used 14-MeV neutrons in preliminary experiments devoted to irradiation of *fissile materials* (*Fuel assembly EK-10*).

We have provided our experiments in the same geometry as it is presented in Fig. 4. Our preliminary estimations and examination of the above Fig. 5 and 6 as well as our experimental oscilloscope traces from our DPF operated with DT mixture as a working gas gave us the following moments for peaks *expected* in our TOF oscilloscope traces:

1. Main neutron energy peaks from the DPF source originating from D-T nuclear reactions according to our previous measurements: 1-st pulse – 14.0 MeV, 2-nd – 13.7 MeV, 3-rd – 12.5 MeV

2. ${}^{8}_{16}O$ : 12.5; 11.0; 8.0…5.0; 2.5 MeV
3. ${}^{13}_{27}Al$ : 5.5; 4.0; 2.7 MeV
4. ${}^{12}_{24}Mg$ : 12.5; 5.5; 4.0; 2.3; 2.0; 1.8; 1.6 MeV
5. Neutron energy peaks from the DPF source originating from D-D nuclear reactions (having about 2 orders of magnitude lower amplitude compared with the 1st peaks) according to our previous measurements: 2.5…2.7 MeV
6. ${}^{92}_{238}U$ and ${}^{92}_{235}U$ : 12.7; 3.5…(1.5-1.0)…0.5 MeV.

One may see that some of the above-mentioned peaks are overlap.

Taking into consideration that the hard X-Ray peak is generated inside the DPF chamber about 10-20 ns earlier compared with the maximum of the main pulse of 14-MeV neutrons we estimate positions of the most important pulses in the TOF oscilloscope traces estimated (recalculated from the above energies to time of flight) – for PMT+S detector placed at the distance 6 m in this case:

- HXR top – 0 ns,
- 14-MeV (direct) neutrons – 115 ns,
- 3-MeV D-D and elastically scattered neutrons – 250 ns,
- 1.5 MeV – 350 ns, 1.0-MeV – 433 ns, 0.5-MeV – 618 ns (fission neutrons),

and we found that these peaks in the oscilloscope traces of Fig. 13 and 14 are coincided with the above estimations and as well as with our modelling simulations presented in Fig. 6.

We have to mention here that one may see several additional peaks on the oscilloscope traces having nothing with our object under interrogation. They results from the neutron elastic scattering due to various elements of our DPF device such as DPF chamber (Cu), current collector (Cu), 4 transformers, 4 capacitors filled with castor oil, polyethylene and Teflon plates, cables, etc. They are positioned on different distances from the neutron source (usually further compared with the position of our bottle) and at dissimilar angles. However we know where we have to expect *the peaks of our interest* in the oscilloscope traces (usually first pulses of the chain) beforehand, and we found them namely in these time positions. Fortunately in this case we have no overlapping of these peaks with peaks from other elements as it was proved by the amplitude analysis.

e. Now it is interesting to understand *how many scattered neutrons can reach and can be captured by our scintillator*. Let us make estimations for the most doubtful case of scintillator having 50 cm in diameter and 50 cm by length when DPF irradiate only $10^8$ 2.45-MeV neutrons per pulse (case ***b***)). From geometry of the experiment it is easy to calculate that our bottle (10 cm in diameter and 15 cm by height placed at a distance 7.75 cm) encompasses ~1/7 part of the solid angle thus giving a figure for total number of neutrons irradiated it equal to about 14%. The above-mentioned cross-sections give evidence that the majority of neutrons coming to the bottle will be scattered by it. It means that the total number of scattered neutrons will be: $10^8 \times 0.17 \cong 1.7 \times 10^7$. At the distance of 2.2 meters where we have our S+PMT-1 the neutron flux density will be equal to 25 n/cm$^2$.

Taking into consideration that the neutron-receiving surface of the scintillator is $2 \times 10^3$ cm$^2$ and that almost a half of our neutrons ($E_n$ ~ 2.5 MeV) will be captured by the scintillator of this thickness we obtain for the number of neutrons forming two our pulses (scattered by O and N nuclei) the figure more than $10^5$ neutrons (note that nuclei of hydrogen do not scatter neutrons in this our geometry). This is a reasonable body for the two pulses of acceptable quality (i.e. we obtain rather good statistics).

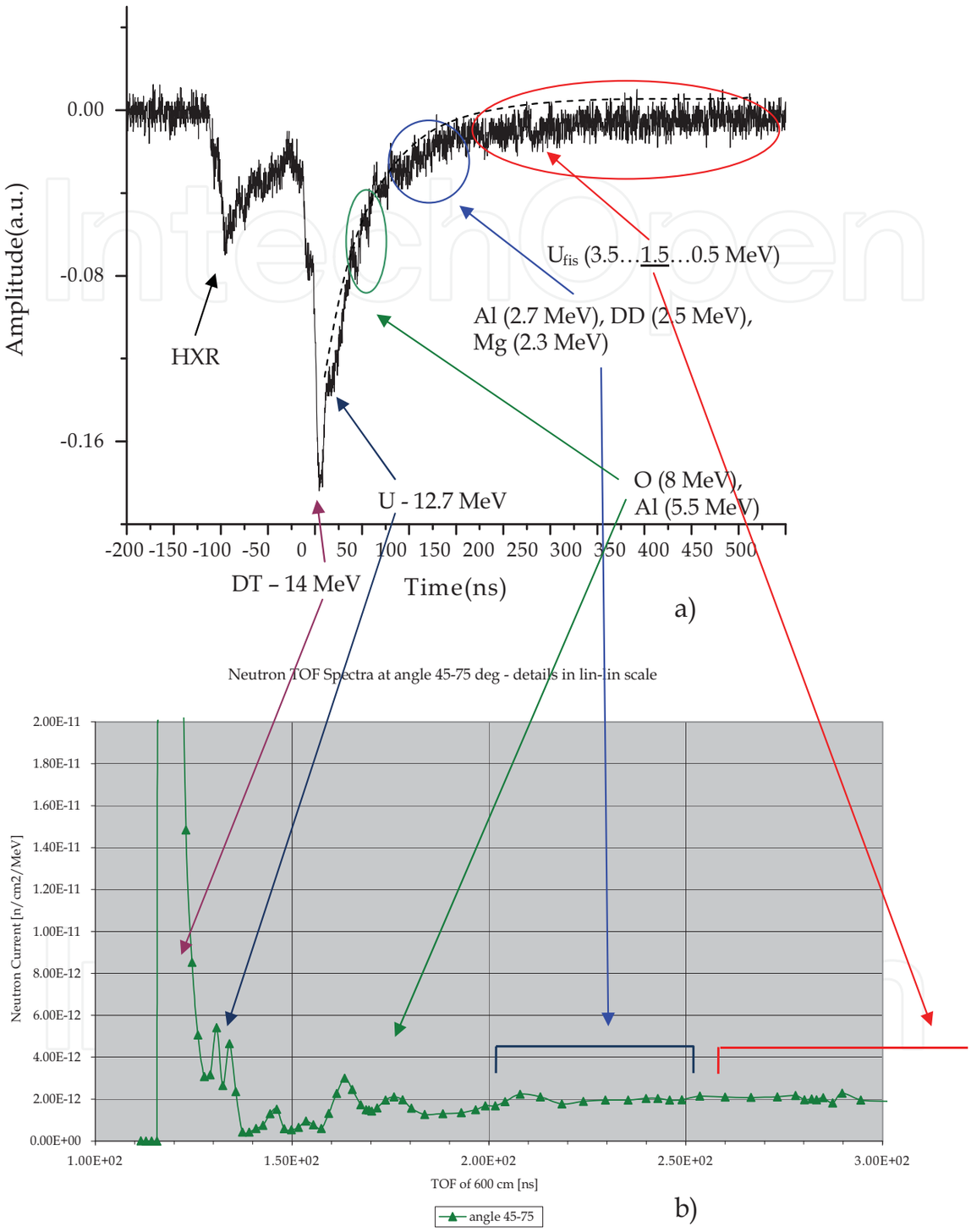


Fig. 13. Experimental oscilloscope traces (*a*) showing: 1) peaks of neutrons scattered by nuclei composing fission fuel element (U, O, Mg, Al); 2) sufficiently broader peak around 1.5 MeV belonging to fission neutrons; and 3) their comparison with numerical modelling made with the help of FLUKA code (*b*)

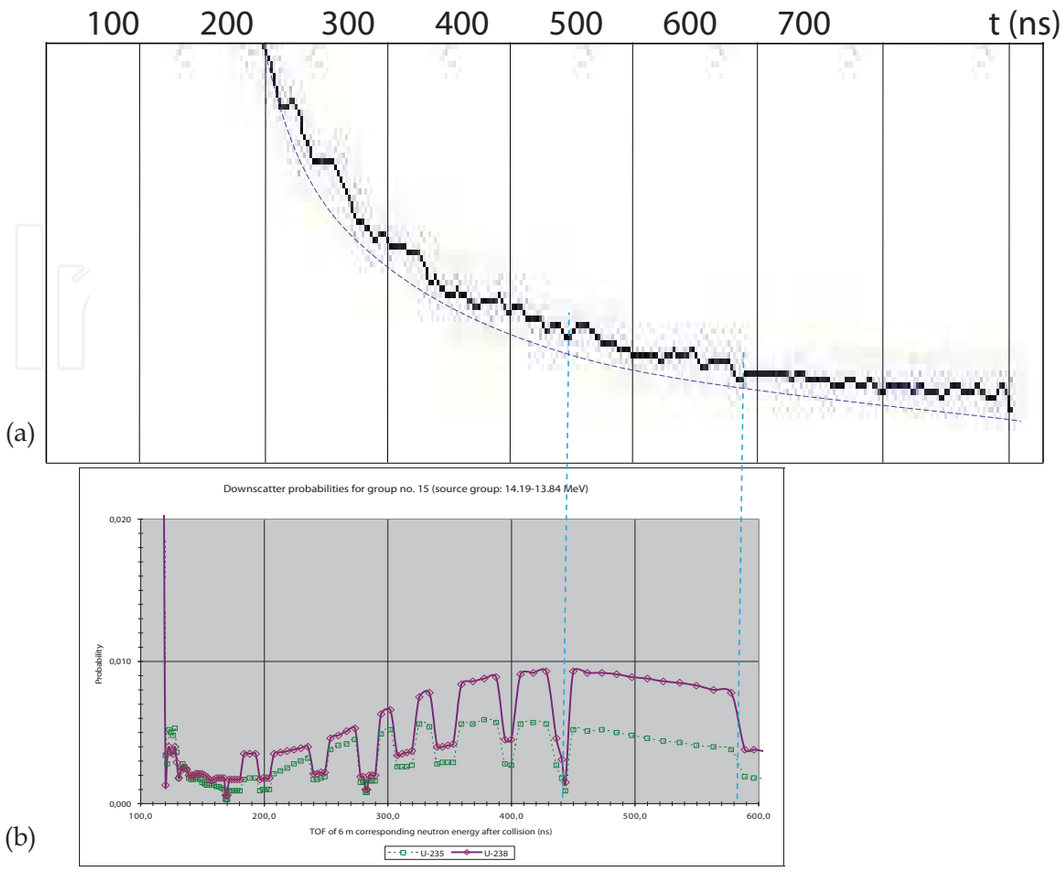


Fig. 14. Part of the oscilloscope trace related to the spectrum range of inelastically scattered by nuclei of U-235 and U-238 (i.e. fission) neutrons cleaned from noises by a Wavelet technique in relation to the TOF signal calculated by FLUKA code

f. Restrictions of the method

The method proposed has of course some restrictions. As it was shown in many works all explosive substances have in their contents hydrogen (a.w. = 1), carbon (a.w. = 12), nitrogen (a.w. = 14), oxygen (a.w. = 16) (and sometimes potassium (a.w. = 39). At the same time the main feature, which differs explosives from another substances, is *the almost equal percentage* of the above 4 main elements (H, C, O, and N) within them in contrast to common materials (see e.g. [1]). It means that taking into account cross-sections of elastic scattering of neutrons by the above nuclei we can expect the *predictable* (almost equal) amplitudes of the three peaks of neutrons scattered backward from C, O, N and separated one from another by the *predictable* time-delays as well as one peak of about the same amplitude scattered forward from H nuclei (at a proper choice of the scattering angles). Namely, presence of these 4 peaks at two PMT' oscilloscope traces will be a "signature" of an explosive in a box under interrogation.

Of course it is possible that some other elements positioned at another distance (and/or at another angle) may give a scattering peak, which overlap one of our peaks. In these circumstances still we shall have 3 suspicious peaks yet of distorted amplitudes. This is one of the restrictions of the method. However in this case we may repeat our shot making it at a different angle (rotating the object under interrogation). After this procedure we shall

distinguish our peaks perfectly. Or we may use the 3-rd (or even 4-th) PMT+S placing it at a different angle to an object. Then we may compare our suspicious peaks *in the same shot*.

g. Perspectives

We believe that the perspectives of the NINIS method (an increase of its reliability in unveiling of illicit items and a decrease of its fault preditions) lie in the following additional techniques that may be exploited in the same single shot of the DPF device:

- use of both 2.45- and 14-MeV neutrons simultaneously (i.e. in filling of DPF by DT-mixture as a working gas) with measurements of elastically scattered neutrons of *both* energies,
- in measurements (additionally to scattered neutrons) of the *characteristic photons* appeared due to $(n,\gamma)$ inelastic neutron scattering (both prompt and delayed),
- in application of hard X-Ray *imaging* of an object during the same DPF shot by use of an X-Ray flash produced by DPF (see e.g. Fig. 8),
- in elaboration of *automated* (computer-aided) procedure of the identification of chemical content of details (sub-items) of an object using X-Ray image in combination with data obtained from elastically and inelastically scattered neutrons and photons $(n,\gamma)$ appeared due to $(n,\gamma)$ inelastic neutron scattering in the same single DPF shot, and
- in exploiting of the fact that the spatial size ("thickness" of the neutron shell irradiated by a DPF device) is in the range 10…50 cm for an interrogation of large (e.g. sea containers) objects; having as a monitor the PMT+S system we shall know precisely at each moment the *configuration of our neutron shell* spreading inside the item, i.e. we shall know the distance between scatterers (elements inside the container) and the neutron source; it will give us an opportunity for identification of every pulse of scattered neutrons in the manner described above; use of a couple of 2D matrix of the PMTs ensures a characterization of the suspicious large-scale object with a spatial precision ("voxel") of the above-mentioned 10...50 cm.

However this *single-shot nanosecond technique* gives something more (as it was mentioned in the preface). We believe that this feature is very important and forms for NINIS its special niche between other methods. We mean the following aspect of the method. If a car of a suicide bomber fully loaded with explosives moves to its target with the speed 100 km per hour (as it happened by the spring of the year 2009 during the attempt on the life of the president of Ingushetia Yunus-Beck Evkurov in southern Russia) it passes during our *10-ns* neutron pulse a distance equal to 1 micrometer only. Thus for a DPF's neutron pulse it is a *static* object. Such a car can be interrogated and eliminated *before* it strikes the goal. Same opportunity may be important for interrogation of a train during its movement.

Second unique opportunity is connected with the fissile materials. Being almost monochromatic the nanosecond pulses of neutrons with energy around 2.45 MeV (for DD reactions) or 14.0 MeV (for DT reactions) irradiated by DPF may unveil these substances practically instantly with the distance of irradiation of a suspicious object from the DPF chamber just of the order of a meter. In this method fast measurements of both over-running neutrons and specific features of the induced fission neutron spectrum may be used.

Third opportunity is connected with the low-dose aspect of the NINIS technique. It is easy to estimate that at the pulse with the total number of 2.45-MeV neutrons equal to $10^9$ per shot (which is perfect for NINIS) an object (e.g. a suicide bomber) at the airport standing at a distance of 1 meter from the DPF chamber and having a half-square-meter area will obtain a dose equal to a three-days background irradiation on the Earth surface or a dose equal to those absorbed by him during his planned flight.

## 4. Pulsed neutron source for Boron Neutron Capture Therapy - initial simulation results

The use of short and powerful neutron pulses for Boron Neutron Capture Therapy (BNCT) potentially could reduce the total dose absorbed by the patient. A Dense Plasma Focus device (DPF) emits very short (in the nanosecond range) and extremely intense pulses of X-Rays and fast neutrons (2.5- or 14-MeV neutrons energy from D-D or D-T nuclear reactions respectively). It was demonstrated that interaction of very powerful beam of X-Rays with bio-test objects during few nanoseconds can produce diverse effects on the biochemical functions of the cells [7]. The induction of the synergetic effects within the cells, e.g. producing a high concentration of secondary particles (free radicals, ions, and electrons) during a time interval short compared with the periods of durations of chemical reactions with the above particles, may result in a collective action of them.
Nevertheless there is no evidence up to now of the use of pulse neutron flash in BNCT, but it is known [8] that the use of nanosecond X-Ray pulses in radiation chemistry and biology could produce the desiderate effect with a considerable less total absorbed dose. At the same time in the work [9] it was shown that spectrum of neutrons where not only thermal but also fast neutron component is presented improves cancer treatment. From the other side in the paper [10] it was studied a possibility of using pulsed radiation of high-power in biological applications and its potential advantages.
The biological effects of radiation depend on the dose, the dose power and the spatial distribution of the microscopic energy deposition. To verify the recent studies of the interactions of pulsed radiation with biological tissues [11] in the context of BNCT treatment, we introduced in our model the effects of the temporal profile of the beam (pulsed versus continuous radiation).
In this work we focus on the development of a detailed simulation of interaction of short-pulse radiation generated by a DPF with tissue to estimate the absorbed dose by the cells for this dynamic case. The simulation was carried out by means of the Geant4 code [12], a toolkit to simulate the interaction of radiation with matter, originally developed for nuclear and particle physics. The experimental simulation was developed in three fundamental steps. The first consists in the modeling of the pulsed neutron source itself. The second is devoted to modeling of the interaction of fast mono-energetic neutrons with a moderator specific for BNCT. The third one is the development of a biological model to quantify the interaction of the pulsed neutron beam with a tissue.

### 4.1 Model

The simulation process includes: geometry of the system, materials involved, and physical processes governing particle interactions.
In the first stage a DPF was simulated. Using the Geant4 for the simulation of the system geometry, DPF was implemented following the features for the DPF construction (Fig. 15). The neutron source was taken with neutrons produced from the D-D reaction, i.e. with energy E = 2.45 MeV, and it had a flux $\Phi=10^9$ neutron/cm$^2$ on the wall of the discharge chamber of a DPF. It means that the overall neutron yield of the device is about $10^{12}$ neutrons/pulse in full solid angle. Several such DPF devices were in operation since the beginning of 70's [13]. With a present day technology [14] such neutron yield may be generated by this device having energy in their capacitor bank about 100…200 kJ, current on the level of 2.5…3 MA and with a footprint of the device (including its battery) about 5 m$^2$. In the case when a D-T mixture is used as a working gas this device may produce a flash of 14-MeV neutrons with the yield two orders of magnitude higher compared with pure deuterium working gas [15].

In the Geant4 model, the pulsed neutron radiation was generated. The specific capability of G4 to keep track of temporal evolution of the different processes was used to verify the temporal evolution signature of short neutron pulses at different distances from the source.

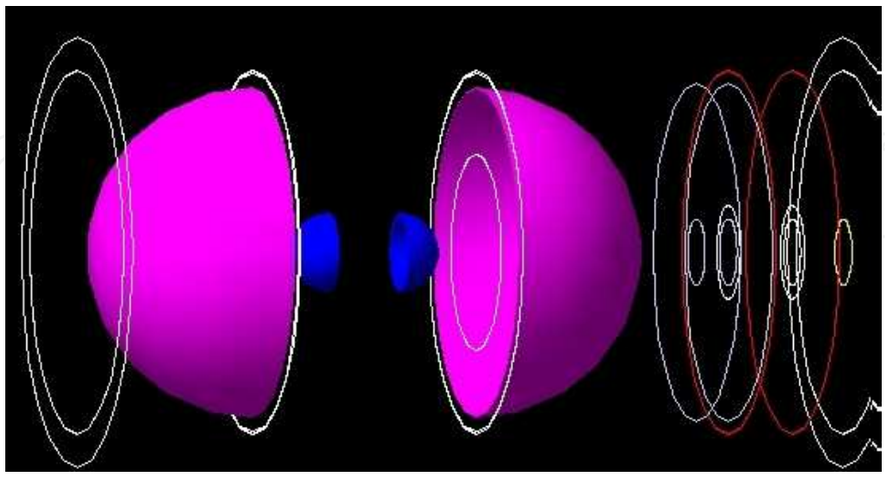

Fig. 15. Plasma Focus Device geometry simulated in Geant4. The internal diameter of the spherical anode (blue) of the device's chamber is 60 mm. The external diameter of the spherical cathode (pink) of the device's chamber is 120 mm

Important problem arising at the interaction of powerful pulses of neutrons with living tissues is the time duration of their interaction. In real experiment it has to depend on neutron interaction process with a moderator (second step) and then with a human phantom (third stage).

Neutron thermalization was studied in detail. For this case, a point neutron source surrounded by a water sphere with 0.5 cm radius was considered. An energy detector was placed at the sphere surface. The resulting neutron spectrum was calculated and subsequently used in the simulation of the interaction process of them with the cells cluster at the second stage of our computing.

This model includes also the development of a human phantom placed at 3 meters from the pulsed neutron source, and the evaluation of Dose deposition in a phantom produced by each neutron pulse. The energy deposition is found placing a detector in the phantom to measure the energy deposited in the body.

Another set of calculations was provided for the special case where we tried to preserve as much as possible the short duration of the neutron pulse generated by a DPF.

These neutrons (D–D fusion neutrons with energy of 2.45 MeV and D–T fusion neutrons with energy of 14 MeV) need to be moderated to the optimal neutron energy spectrum for BNCT. Moderating the neutrons to near the optimal energy of 10 keV [16] can be performed in two stages. In the above-mentioned study [16] the best results were achieved with iron and Fluental™ moderator materials. Fluental™ (69% AlF3/30% Al/1% LiF) is a neutron moderator material developed at VTT in Finland. The material combination of Fluental™ is ideal to decrease the neutron flux to the desired energy range of 10 keV without over-moderation. This particular energy (10 keV) is good for cancer therapy from three points of view – relatively long penetration depth of these neutrons into human body (a few cm), favorite (as it was shown in [9]) neutron spectrum enriched by fast neutrons, and still a high cross-section of neutrons' absorption by boron nuclei (for applicability of BNCT). In Fig. 16 we present geometry of our moderator's assembly.

Fig. 16. Moderator's assembly: copper layers (white), Fluental™ material (blue), iron (yellow), plasma column, producing neutrons inside the DPF discharge chamber (red)

However a problem is raised here: whether this moderation process (being in any case much more preferable in comparison with moderation by hydrogen-containing substances like water) will preserve the pulse duration $\tau$ of the neutron radiation from DPF still much shorter than the duration of reactions with e.g. free radicals (i.e. $\tau << 1$ μs)?

### 4.2 Geometry of the modeled cell's cluster

A closed packed structure of 14 spheres made from homogeneous material, whose composition was defined using the parameters of table (1) from ICRU [11] was used. The arrangement of the cells in the cluster was optimized to use less space [17] (see Fig. 17). Each cell had a diameter of 13 μm. The cell composition used in our model was that defined by ICRU [11] (table1), but we included a Boron with the concentration of 30 ppm of boron nuclei per tissue's molecules.

| Composition of the Cell Medium | | | | | | |
|---|---|---|---|---|---|---|
| | Hydrogen | Carbon | Nitrogen | Oxygen | Phosphorus | Boron |
| Tissue | 59.59 % | 11.109 % | 4.039 % | 24.239 % | 1.009 % | 0.0029 % |

Table 1.

### 4.3 Dose distribution and number of tracks through the cluster

Geant4 calculates the neutron interaction with the cell's atoms using a Monte Carlo algorithm and tracks of the resultant particles produced by the nuclear reactions, including also the secondary reactions of the resultant's particles. The energy deposition is found placing a detector in the cytoplasm to measure the energy deposited in the cell. The dose (in Grays) and the mean track length of the particles (in micrometers) are then evaluated.

### 4.4 Results

In this section we present general results obtained with our simulations.

The pulsed simulated neutron spectrum was calculated with its initial time spread of 10 ns. Its moderated spectrum was found in general agreement with the predictions, given the amount of moderation material in front of the neutron source. The relative amount of quasi-thermal neutrons (with energy less than 1 MeV) was found to increase with the amount of

fluental material. A preliminary tradeoff of the desired neutron spectrum with the optimal pulse spread was calculated.

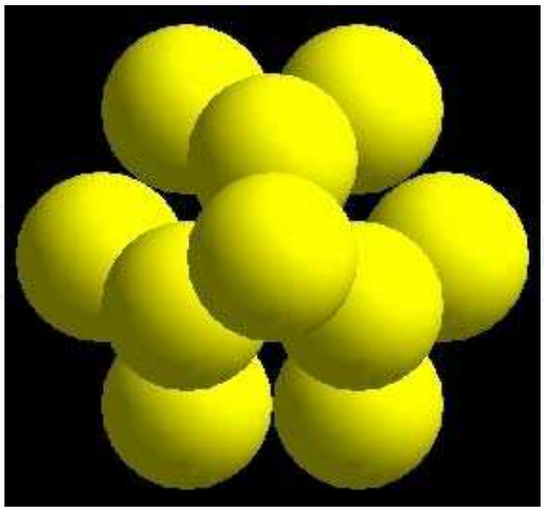

Fig. 17. Image of cell cluster as simulated by G4. Dimension of the cell cluster is around 26 μm of diameter, arranged in order to minimize the space by each cell. The cells in the cluster were surrounding by water

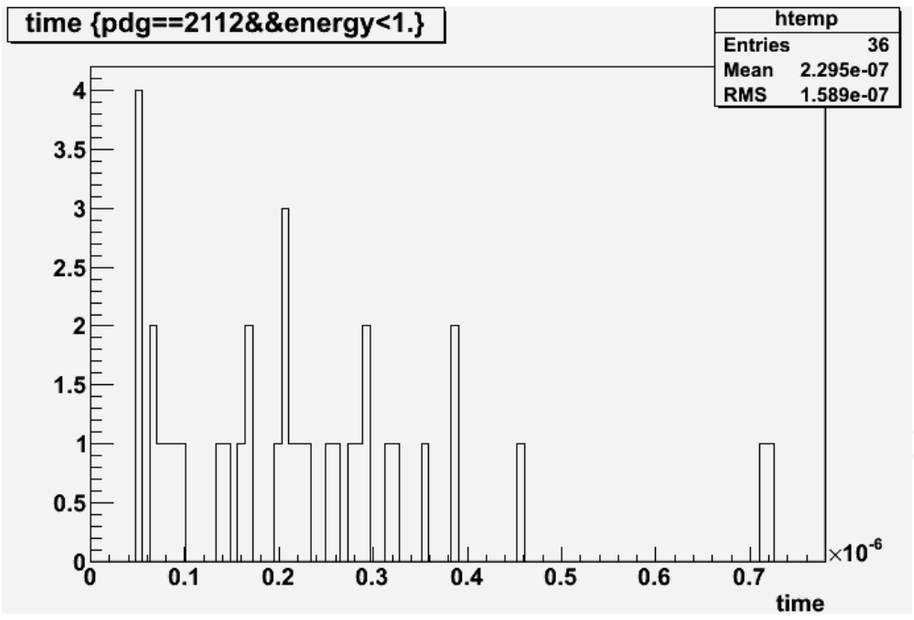


Fig. 18. Temporal shape of a 50-ns pulse of 2.5-MeV neutrons after its moderation by means of the assembly shown in Fig. 16

Similar studies were performed with a large iron/fluental moderator (see Fig. 16), where a larger moderation is obtained while keeping the neutron pulse within the time scale much less than 1 microsecond. The resulting spectrum was found to be much more thermal than the previous one. In these calculations we used a 50-ns neutron pulse. The final pulse shape width (FWHM) was found to be 200 nanoseconds, only a factor of 4 more than the initial neutron pulse width (see Fig. 18).

The resulting spectrum is then moderated by a large water sphere to simulate an isotropic flux as the one delivered to treated cells. The dose delivered to small cells was then preliminary evaluated. First, we have found that the dose is distributed homogeneously among the cells within the cluster. Second, we found small differences in dose deposition between the cells of the cluster. These differences arise mostly from the differences in a number of tracks through each cell; therefore the number of neutrons will be more important in determining the number of tracks through the cells rather than the energy of the neutrons. The preliminary results we obtained at this level need to be validated since the ability of Geant4 to track neutrons inside the cell cluster at such small scales has to be demonstrated. We will plan dedicated measurements to validate our results. The result from this model suggests that one should plan the *in vitro* experiment in mammalian cells using pulsed neutron source taking into account that the dose deposition will be homogeneously distributed around tissue.

## 5. Acknowledgments

The work was partly supported by grants from: Polish Ministry of Science and Higher Education No. O N202 049735 and from NATO Science for Peace Programme, SfP-981118.

## 6. References

[1] J. Csikai "Neutron-based techniques for the detection of concealed objects", *Proc. of the enlargement workshop on "Neutron Measurements and Evaluations for Applications"*, 5-8 November 2003, Budapest, Hungary, Report EUR 21100 EN

[2] A.M. Pollard, C. Heron, Archaeological chemistry, Cambridge, Royal Society of Chemistry (1996)

[3] a) F.D. Brooks, A. Buffler, M.S. Allie, K. Bharuth-Ram, M.R. Nchodu and B.R.S. Simpson "Determination of HCNO concentrations by fast neutron scattering analysis", *Nuclear Instruments and Methods in Physics Research* A 410 (1998) 319 – 328

b) G. Nebbia, S. Pesente, M. Lunardron, S. Moretto, G. Viesti "Use of neutron based technique in the control of illicit trafficking of fissile and explosive material", *S. Apikyan and D. Diamond (eds.), Countering Nuclear and Radiological Terrorism,* 271-290 (2006) Springer, Printed in the Netherlands

c) Yigang Yang, Yuanjing Li, Haidong Wang, et al. "Explosives detection using photoneutrons produced by X-rays", *Nuclear Instruments and Methods in Physics Research* A 579 (2007) 400–403

d) Kiyoshi Yoshikawa, Kai Masuda, Teruhisa Takamatsu, Seiji Shiroya, Tsuyoshi Misawa, Eiki Hotta, Masami Ohnishi, Kunihito Yamauchi, Hodaka Osawa, Yoshiyuki Takahashi "Research and development of a compact discharge-driven D–D fusion neutron source for explosive detection" *Nuclear Instruments and Methods in Physics Research* B 261 (2007) 299–302

e) E.T.H. Clifford, J.E. McFee, H. Ing, H.R. Andrews, D. Tennant, E. Harper, A.A. Faust "A militarily fielded thermal neutron activation sensor for landmine detection", *Nuclear Instruments and Methods in Physics Research* A 579 (2007) 418–425

f) G. Vourvopoulos, P. C. Womble "Pulsed fast/thermal neutron analysis: A Technique for Explosives Detection"; www.wku.edu/API/research/explo.htm - PELAN

g) "GIOS: Gerät zur Identifizierung Organischer Substanzen", I.U.T. (Institut für Umwelttechnologien) GmbH (brochure); http://www.iut-berlin.de/

[4] a) MCNP – A General Monte Carlo N-Particle Transport Code, Version 5, X-5 Monte Carlo Team, Diagnostics Applications Group, Los Alamos National Laboratory, "MCNP Homepage", http://mcnp-green.lanl.gov/index.html
b) „MCNP5 Homepage", http://mcnp-green.lanl.gov/about_mcnp5.html
[5] a) G. Battistoni, S. Muraro, P.R. Sala, F. Cerutti, A. Ferrari, S. Roesler, A. Fasso`, J. Ranft, "The FLUKA code: Description and benchmarking", *Proceedings of the Hadronic Shower Simulation Workshop 2006*, Fermilab 6--8 September 2006, M. Albrow, R. Raja eds., AIP Conference Proceeding 896, 31-49, (2007)
b) A. Fasso`, A. Ferrari, J. Ranft, and P.R. Sala, "FLUKA: a multi-particle transport code", CERN-2005-10 (2005), INFN/TC_05/11, SLAC-R-773
c) "FLUKA Homepage", http://www.fluka.org/fluka.php
[6] a) V.A. Gribkov, R. Miklaszewski "On a possibility of the single-shot detection of hidden objects by using nanosecond impulse neutron inspection system", *Acta Phys. Chim. Debr*. XXXVIII-XXXIX (2005) 185-193
b) V.A. Gribkov, R.A. Miklaszewski "Nanosecond Radiation Pulses for Rapid Detection of Explosives", *"Combined Devices for Humanitarian Demining and Explosives Detection"*, http://www-pub.iaea.org/MTCD/publications/PDF/Pub1300_label.pdf, *Proc. of an IAEA Tech. Meeting, Padova,* 2006, IAEA-TM-29225, A-03
[7] V.A. Gribkov, M.A. Orlova, "Enzyme Activation and Inactivation Induced by Low Doses of Irradiation", *Applied Biochemistry and Biotechnology*, vol. 88, pp. 243-255, 2000
[8] V.A. Gribkov, A.V. Dubrovsky, M.A. Orlova, M. Scholz, "Opportunities Afforded by New Generation of Pulsed Radiation Sources in Flash Radiation Physics and Chemistry", *Research Journal of Chemistry and Environment*, vol. 9 (4), Dec., pp. 11-19, 2005
[9] T.A. Buchholz , J.S. Rasey, G.E. Laramore, J. Livesey, L. Chin, R. Reisler, A. Spence, T.W Griffin, "Concomitant boron neutron capture therapy during *in vivo* fast neutron radiation of a rat glioma", *Radiology,* 191 (3) (1994) 863–867
[10] V. A. Gribkov, A. V. Dubrovsky, M. Scholz, et al., "PF-6 – an effective plasma focus as a source of ionizing radiation and plasma streams for application in material technology, biology and medicine", *Nucleonika*, 51, No.1 (2006) 55-62
[11] ICRU, Tissue Substitutes in Radiation Dosimetry and Measurements, Report 44, International Commission on Radiation Units and Measurements, Bethesda, MD, 1989
[12] A. Agostinelli et al., "Geant4 – a simulation toolkit", *Nuclear Instruments and Methods in Physics Research,* A 506 (2003) 250-303
[13] A. Bernard et al., "Scientific status of plasma focus research", *Journal of the Moscow Phys. Soc.*, 8, No. 2 (1998) 93-170
[14] V.A. Gribkov, L. Karpinski, P. Strzyzewski, M. Scholz, A. Dubrovsky, "New efficient low-energy dense plasma focus in IPPLM", *Czechoslovak Journal of Physics*, 54, Suppl. C (2004) C191-C197
[15] a) V.P. Vyskubov, V.A. Gribkov, L.M. Zhogov et al., "On the DPF Operation with the D-T Mixture", *P.N. Lebedev Physical Institute Reports*, M: FIAN, No. 12 (1979) 37-41
b) All-Russia Research Institute of Automatics (VNIIA), "VNIIA homepage": http://www.vniia.ru
[16] H. Koivunoroa, D.L. Bleuela, U. Nastasib, et al., "BNCT dose distribution in liver with epithermal D–D and D–T fusion-based neutron beams", *Applied Radiation and Isotopes*, 61 (2004) 853–859
[17] V.J. Petteri, L. Juha, K. Antti, I. Sami, S. Jiri, S. Sauli, "Comparison of different cell-cluster models for cell-level dosimetry", *Acta oncologica*, 40, No. 1 (2001) 92-97


**Applications of Monte Carlo Methods in Biology, Medicine and Other Fields of Science**

Edited by Prof. Charles J. Mode

ISBN 978-953-307-427-6
Hard cover, 424 pages
**Publisher** InTech
**Published online** 28, February, 2011
**Published in print edition** February, 2011

This volume is an eclectic mix of applications of Monte Carlo methods in many fields of research should not be surprising, because of the ubiquitous use of these methods in many fields of human endeavor. In an attempt to focus attention on a manageable set of applications, the main thrust of this book is to emphasize applications of Monte Carlo simulation methods in biology and medicine.

**How to reference**

In order to correctly reference this scholarly work, feel free to copy and paste the following:

V.A. Gribkov, S.V. Latyshev, R.A. Miklaszewski, M. Chernyshova, R. Prokopowicz, M. Scholz, K. Drozdowicz, U. Wiącek, B. Gabańska, D. Dworak, K. Pytel, A. Zawadka, M. Ramos Aruca, F. Longo, G. Giannini and C. Tuniz (2011). Monte Carlo Simulations of Powerful Neutron Interaction with Matter for the Goals of Disclosure of Hidden Explosives and Fissile Materials and for Treatment of Cancer Diseases versus their Experimental Verifications, Applications of Monte Carlo Methods in Biology, Medicine and Other Fields of Science, Prof. Charles J. Mode (Ed.), ISBN: 978-953-307-427-6, InTech, Available from: http://www.intechopen.com/books/applications-of-monte-carlo-methods-in-biology-medicine-and-other-fields-of-science/monte-carlo-simulations-of-powerful-neutron-interaction-with-matter-for-the-goals-of-disclosure-of-h

INTECH
open science | open minds

**InTech Europe**
University Campus STeP Ri
Slavka Krautzeka 83/A
51000 Rijeka, Croatia
Phone: +385 (51) 770 447
Fax: +385 (51) 686 166
www.intechopen.com

**InTech China**
Unit 405, Office Block, Hotel Equatorial Shanghai
No.65, Yan An Road (West), Shanghai, 200040, China
中国上海市延安西路65号上海国际贵都大饭店办公楼405单元
Phone: +86-21-62489820
Fax: +86-21-62489821

IntechOpen